Particle number concentrations and size distributions in the stratosphere: Implications of nucleation mechanisms and particle microphysics

Fangqun Yu[1], Gan Luo[1], Arshad Arjunan Nair[1], Sebastian Eastham[2, 3], Christina J. Williamson[4, 5, a], Agnieszka Kupc[5, 6], and Charles A. Brock[5]

[1] Atmospheric Sciences Research Center, University at Albany, Albany, New York, US

[2] Laboratory for Aviation and the Environment, Department of Aeronautics and Astronautics, Massachusetts Institute of Technology, Cambridge, MA 02139, USA

[3] Joint Program on the Science and Policy of Global Change, Massachusetts Institute of Technology, Cambridge, MA 02139, USA

[4] Cooperative Institute for Research in Environmental Sciences, University of Colorado, Boulder, CO 80309, USA

[5] Chemical Sciences Laboratory, National Oceanic and Atmospheric Administration, Boulder, CO 80305, USA

[6] Faculty of Physics, Aerosol Physics and Environmental Physics, University of Vienna, 1090 Vienna, Austria

[a] now at: Climate Research Programme, Finnish Meteorological Institute, 00101 Helsinki, Finland and Institute for Atmospheric and Earth System Research/Physics, Faculty of Science, University of Helsinki, 00014 Helsinki, Finland.

Correspondence to: F. Yu (fyu@albany.edu)

Abstract. While formation and growth of particles in the troposphere have been extensively studied in the past two decades, very limited efforts have been devoted to understanding these in the stratosphere. Here we use both Cosmics Leaving OUtdoor Droplets (CLOUD) laboratory measurements taken under very low temperatures (205–223K) and Atmospheric Tomography Mission (ATom) in-situ observations of particle number size distributions (PNSD) down to 3 nm to constrain nucleation mechanisms and to evaluate model simulated particle size distributions in the lowermost stratosphere (LMS). We show that the binary homogenous nucleation (BHN) scheme used in most of the existing stratospheric aerosol injection (a proposed method of solar radiation modification) modeling studies overpredict the nucleation rates by 3–4 orders of

31 magnitude (when compared to CLOUD data) and particle number concentrations in the
32 background LMS by a factor ~2–4 (when compared to ATom data). Based on a recently developed
33 kinetic nucleation model, which gives rates of both ion-mediated nucleation (IMN) and BHN at
34 low temperatures in good agreement with CLOUD measurements, both BHN and IMN occur in
35 the stratosphere. However, IMN rates are generally more than one order of magnitude higher than
36 BHN rates and thus dominate nucleation in the background stratosphere. In the Southern
37 Hemisphere (SH) LMS with minimum influence of anthropogenic emissions, our analysis shows
38 that ATom measured PNSDs generally have four apparent modes. The model captures reasonably
39 well the two modes (Aitken mode and the first accumulation mode) with the highest number
40 concentrations and the size-dependent standard deviations. However, the model misses an apparent
41 second accumulation mode peaking around 300–400 nm, which is in the size range important for
42 aerosol direct radiative forcing. The bi-modal structure of accumulation mode particles has also
43 been observed in the stratosphere well above tropopause and in the volcano-perturbed stratosphere.
44 We suggest that this bi-modal structure may be caused by the effect of charges on coagulation and
45 growth, which is not yet considered in any existing models and may be important in the
46 stratosphere due to high ionization rates and long lifetime of aerosols. Considering the importance
47 of accurate PNSDs for projecting realistic radiation forcing response to stratospheric aerosol
48 injection (SAI), it is essential to understand and incorporate such potentially important processes
49 in SAI model simulations and carry out further research to find out what other processes that the
50 present models might have missed.

51

52

53

1. Introduction

Solar radiation modification (also known as solar geoengineering) approaches are being developed in response to the climate crisis (IPCC, 2021). They would temporarily offset climate change by reducing incoming sunlight, augmenting (currently inadequate) mitigation efforts and buying time to reduce atmospheric levels of CO_2, which is the root cause of the climate crisis. A recent report by the National Academies of Sciences, Engineering and Medicine (NASEM) emphasizes the urgent need to have a comprehensive understanding of the feasibility and potential risks/benefits of solar climate intervention approaches (NASEM, 2021). Stratospheric aerosol injection (SAI) has demonstrated the most promise as proximately engineerable (Shepherd et al., 2009; Lockley et al., 2020; IPCC, 2021) and has been extensively studied using models (e.g., GeoMIP: Kravitz et al., 2011; GLENS: Mills et al., 2017; Richter et al., 2022). The NASEM report (NASEM, 2021) pointed out that "the overall magnitude and spatial distribution of the forcing produced by SAI depends strongly on the aerosol size distribution" and "One of the research priorities for SAI is thus to address critical gaps in knowledge about the evolution of the aerosol particle size distribution". In the stratosphere, sulfate aerosols are formed by nucleation, followed by condensational growth and coagulation, and lost by evaporation in the upper stratosphere and downward sedimentation into the troposphere (Turco et al., 1982). New particle formation (NPF) (or nucleation) affects not only the number abundance but also the size distributions of stratospheric particles (e.g., Brock et al., 1995; Lee et al., 2003). There is increasing evidence (Weisenstein et al., 2022, Laakso et al., 2022) that a careful treatment of microphysical processes is necessary for projecting realistic radiative forcing response to SAI.

The process of NPF under tropospheric conditions has been extensively explored over the last two decades through laboratory and field measurements, theoretical studies, and numerical simulations (e.g., Yu and Turco, 2000; Vehkamäki et al., 2002; Kulmala et al., 2004; Kirkby et al., 2011; Dawson et al., 2012; Zhang et al., 2012; Kürten et al., 2016; Yu et al., 2018; Kerminen et al., 2018; Lee et al., 2019). Although some of the advances in our understanding of nucleation gained in the last two decades can be applied to stratospheric conditions, focused studies specifically examining the mechanisms of NPF under stratospheric conditions are quite limited. Indeed, the H_2SO_4–H_2O binary homogenous nucleation (BHN) parameterization developed two decades ago by Vehkamäki et al. (2002) (named BHN_V2002 thereafter) has been widely used in SAI modeling studies when nucleation process is explicitly considered (e.g., Tilmes et al., 2015; Jones et al., 2021; Weisenstein et al., 2022). Tilmes et al. (2015) described a Geoengineering Model Intercomparison Project (GeoMIP) experiment designed for climate and chemistry models, using the stratospheric aerosol distribution derived from the ECHAM5-HAM microphysical model (Stier et al., 2005) which calculated nucleation rates with the BHN_V2002 scheme. Both models (UKESM1 and CESM2-WACCM6) employed for a recent GeoMIP G6sulfur study (Jones et al., 2021) used the BHN_V2002 scheme. In another recent SAI study based on three interactive stratospheric aerosol microphysics models (Weisenstein et al., 2022), two models (MAECHAM5-HAM and SOCOL-AER) used BHN_V2002 scheme while the other (CESM2-WACCM) used an empirical nucleation scheme to calculate nucleation rate as a function of sulfuric acid concentration only (i.e, no dependence on temperature and relative humidity). To our knowledge, the performance of this widely used BHN_V2002 under stratospheric conditions has not been carefully examined, probably due to the lack of suitable in situ measurements of freshly nucleated particles in the stratosphere for constraining the scheme. In this regard, particle size distributions down to 3 nm measured in-situ during the NASA Atmospheric Tomography Mission (ATom) in

the lowermost stratosphere (LMS) of both SH and NH in four different seasons (Williamson et al., 2019, 2021; Kupc et al., 2020; Brock et al., 2021) provide much-needed data to constrain our understanding of the nucleation and particle microphysics in the stratosphere. In addition, well-controlled CLOUD experiments taken under low temperature (within the range of stratosphere) can also be used to assess the performance of nucleation schemes under stratospheric conditions. Another important issue related to stratospheric particles is the role of ionization in nucleation. It is well established that nucleation of H_2SO_4–H_2O on ions is favored over homogenous nucleation (Hamill et al., 1982; Yu and Turco, 2000; Lovejoy et al., 2004; Kirkby et al. 2011; Yu et al., 2018) but the role of ionization in NPF in the stratosphere has not been considered in any previous SAI studies (to our knowledge) in spite of the very high ionization rates in the stratosphere.

In this study, we use both CLOUD laboratory measurements taken under very low stratospheric temperatures and ATom PNSD measurements in LMS to constrain nucleation mechanisms and model simulated particle size distributions. For 3-D simulation of size-resolved stratospheric aerosols, we use the GEOS-Chem with the unified tropospheric-stratospheric chemistry-transport model with the size-resolved advanced particle microphysics (APM) package.

2. Model and data

2.1 GEOS-Chem/APM

The GEOS-Chem model is a global 3-D model of atmospheric composition (e.g., Bey et al., 2001) and is continuously being improved (e.g., Luo et al., 2020; Holmes et al., 2019; Keller et al., 2014; Murray et al., 2012; Pye and Seinfeld, 2010; van Donkelaar et al., 2008; Evans and Jacob, 2005; Martin et al., 2003). The GEOS-Chem tropospheric–stratospheric unified chemistry extension (UCX; Eastham et al., 2014), now the standard GEOS-Chem configuration, implements stratospheric chemistry, calculation of J-values for shorter wavelengths, and improved modeling of high-altitude aerosols. Extension of the chemistry mechanism to include reactions relevant to the stratosphere enables the capturing of stratospheric responses and troposphere–stratosphere coupling. UCX adds 28 species and 104 kinetic reactions, including 8 heterogeneous reactions, along with 34 photolytic decompositions. Atomic oxygen [both $O(^3P)$ and $O(^1D)$] is explicitly modeled; although also of short lifetime in the stratosphere, these species are important in correctly modeling stratospheric chemistry. Photochemistry is extended up to the stratopause to high-energy photons (177 nm) using the Fast-JX model, which includes cross-section data for many species relevant to the troposphere and stratosphere. Photolysis rates respond to changes in the stratospheric ozone layer. Additional heterogeneous reactions (Kirner et al., 2011, Rotman et al., 2001, Shi et al., 2001) are included to capture seasonal ozone depletion. H_2O is treated as a chemically-active advected tracer within the stratosphere. These permit chemical feedbacks between stratospheric ozone and aerosols and tropospheric photochemistry. The improved GEOS-Chem with coupled stratospheric–tropospheric responses has been evaluated with sonde and satellite measurements of O_3, HNO_3, H_2O, HCl, ClO, NO_2 and stratospheric intrusions (Eastham et al., 2014; Gronoff et al., 2021; Knowland et al., 2022). Yu and Luo (2009) incorporated a size-resolved (sectional) APM package into GEOS-Chem, henceforth referred to as GC-APM. The APM separates secondary particles from primary particles, uses 40 bins to represent secondary particles with high size resolution for the size range important for the growth of nucleated particles to accumulation mode sizes, and contains options to calculate nucleation rates based on different

142 nucleation schemes. In GC-APM, nucleation is calculated before condensation using a time-
143 splitting technique. Therefore, no competition between nucleation and condensation for sulfuric
144 acid vapor is considered. In most conditions, nucleation consumes only a very small fraction (<1%)
145 of sulfuric acid vapor in the air and the time splitting does not affect the results. When nucleation
146 rate is high, reduced time step for nucleation and growth is used to ensure that the fraction of
147 sulfuric acid vapor consumed by nucleation each time step is small. The GC-APM uses a semi-
148 implicit scheme to calculate sulfuric acid condensation together with sulfuric acid gas phase
149 production to ensure that the change of sulfuric acid vapor concentration is smooth. APM is fully
150 coupled with GEOS-Chem in both the troposphere and stratosphere.
151 In the present study we have carried out GEOS-Chem-UCX/APM global simulations from
152 01/2015 to 05/2018, with the first 17 months as spin-up and the remaining period covering ATom
153 1-4 periods (06/2016–05/2018). The horizontal resolution is $4^o \times 5^o$ and there are 72 vertical layers.
154 Emissions from different sources, regions, and species are computed via the Harvard-NASA
155 Emissions Component (HEMCO) on a user-defined grid (Keller et al., 2014). Historical global
156 anthropogenic emissions are based on the Community Emissions Data System (CEDS) inventory
157 (Hoesly et al., 2018). Regional anthropogenic emissions over the United States, Canada, Europe,
158 and East Asia are replaced by regional emission inventories of the National Emissions Inventory
159 (NEI, https://www.epa.gov/air-emissions-inventories/2017-national-emissions-inventory-nei-
160 data), the Air Pollutant Emission Inventory (APEI, https://www.canada.ca/en/environment-
161 climate-change/services/pollutants/air-emissions-inventory-overview.html), the Co-operative
162 Programme for Monitoring and Evaluation of the Long-range Transmission of Air Pollutants in
163 Europe (EMEP, https://www.emep.int/index.html), and the MIX Asian emission inventory (Li et
164 al., 2017), respectively. Monthly mean aircraft emissions are generated based on the Aviation
165 Emissions Inventory v2.0 (Stettler et al., 2011). The aircraft particle emissions include nucleation
166 mode sulfate particles (Emission index = 2×10^{17} /kg-fuel, mean diameter = 9 nm, based on Kärcher
167 et al., 2000), and black carbon and primary organic carbon (POC) particles. Global biomass
168 burning is taken from Global Fire Emissions Database version 4 (van der Werf et al., 2017). The
169 volcanic emissions of SO_2 are taken from AeroCom point-source data (Carn et al., 2015). Fixed
170 global surface boundary conditions are applied for N_2O, CFCs, HCFCs, halons, OCS and long-
171 lived organic chlorine species (Eastham et al., 2014).
172
173 **2.2 Airborne ATom measurements of PNSD**
174 Measurements are essential in advancing our understanding of stratospheric aerosol properties
175 and the fundamental processes governing these properties. NASA's Atmospheric Tomography
176 Mission (ATom; Wofsy et al., 2021; Thompson et al., 2022) is a multi-agency effort that provides
177 global in situ aircraft observations of the vertical structure of aerosols from near surface to ~12 km
178 altitude. PNSDs are measured using the NOAA Aerosol Microphysical Properties (AMP) package
179 (Brock et al., 2019) comprising nucleation-mode aerosol size spectrometer(s) (NMASS)
180 (Williamson et al. 2018), ultra-high-sensitivity aerosol spectrometer(s) (UHSAS) (Kupc et al.
181 2018), and a laser aerosol spectrometer (LAS) covering aerosol sizes from 3 nm to 4.5 μm. The
182 aerosol number abundance can be obtained by integrating the PNSD measurements.
183
184 **2.3 The CLOUD (Cosmics Leaving OUtdoor Droplets) measurements**

185   Laboratory measurements of nucleation rates as a function of key controlled parameters have
186   been carried out in a 26.1 m³ stainless steel cylinder chamber at the European Organization for
187   Nuclear Research (CERN), in the framework of the CLOUD experiment (Cosmics Leaving
188   OUtdoor Droplets) (e.g., Kirkby et al., 2011; Kürten et al., 2016; Dunne et al., 2016). Some of
189   these experiments were conducted at the temperature in the range of those in the stratosphere
190   (Kirkby et al., 2011; Dunne et al., 2016) which are used in this study to evaluate nucleation
191   schemes under stratospheric conditions.
192
193   **3. Results**
194   **3.1 H₂SO₄–H₂O binary homogeneous nucleation (BHN) and binary ion-mediated nucleation**
195   **(BIMN) under stratospheric conditions**
196   Nucleation is one of the microphysical processes influencing particle size distributions in the
197   stratosphere (Turco et al., 1982) The CLOUD measurements under a wide range of well-controlled
198   conditions (Kirkby et al., 2011; Dunne et al., 2016) provide a unique set of data to evaluate the
199   nucleation theories. Yu et al. (2020) compared nucleation rates calculated based on a number of
200   commonly used aerosol nucleation parameterizations with the CLOUD measurements. Here we
201   specifically examine the comparison under stratospheric conditions where temperature is below ~
202   230 K. Since ammonia concentrations in the stratosphere are generally negligible, we focus on
203   binary nucleation in the present study. The contribution of organics to particle formation, growth,
204   and compositions in the upper troposphere and LMS has been investigated in several studies (Kupc
205   et al., 2020; Murphy et al., 2021; Williamson et al., 2021). Because of the lack of information with
206   regard to the low volatile gaseous organic species, the possible role of organics in new particle
207   formation in LWS is not considered in the present study.
208
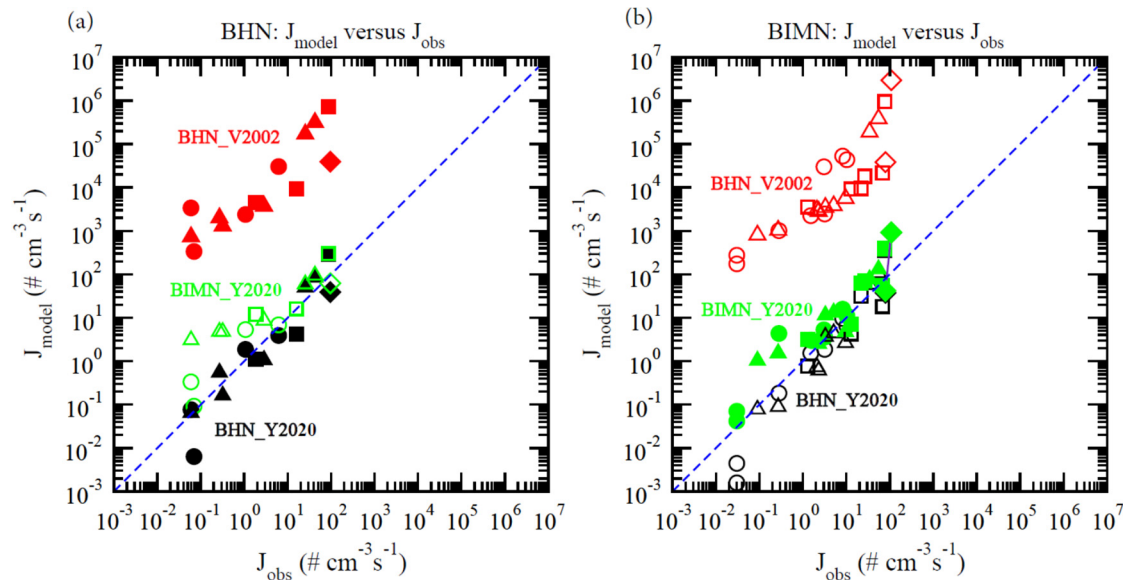
210   **Figure 1.** Comparison of nucleation rates based on three different schemes with CLOUD
211   measurements within the low temperature range (T = 205–223 K) as that in the stratosphere for (a)
212   binary homogeneous nucleation (no ionization) and (b) ion nucleation (at the presence of
213   ionization rates 2.51 – 110 ion-pairs cm⁻³s⁻¹). The different nucleation schemes shown are: BHN
214   of Vehkamäki et al. (2002) (BHN_V2002), BHN of Yu et al. (2020) (BHN_Y2020), and BIMN
215   of Yu et al. (2020) (BIMN_Y2020). For comparison, under binary condition of (a), BIMN rates at

216   $Q = 20$ ion-pairs cm^{-3}s^{-1} are given while under binary ion nucleation condition of (b), BHN rates
217   are also given. Values of H$_2$SO$_4$ vapor concentration ([H$_2$SO$_4$]) range from 10^6 to 3×10^7 cm^{-3} and
218   are separated into four groups in the plots (Circles: $10^6 – 5\times10^6$ cm^{-3}; triangles: $5\times10^6 – 10^7$ cm^{-3};
219   Squares: $10^7 – 1.5\times10^7$ cm^{-3}; Diamonds: $1.5\times10^7 – 3\times10^7$ cm^{-3}).

221   Figure 1 compares nucleation rates based on the following three different schemes with
222   CLOUD measurements under stratospheric temperature range (T = 205–223 K): BHN of
223   Vehkamäki et al. (2002) (BHN_V2002), BHN of Yu et al. (2020) (BHN_Y2020), and BIMN of
224   Yu et al. (2020) (BIMN_Y2020). BHN_V2002 and BHN_Y2020 differ in term of thermodynamic
225   data and nucleation approach used (Yu et al., 2020). To show the relative importance of
226   homogeneous versus ion nucleation, BIMN rates at Q = 20 ion-pairs cm^{-3}s^{-1} were given under
227   binary homogeneous condition in Fig. 1a and BHN rates were also given under binary ion
228   nucleation condition in Fig. 1b. Nucleation rates based on BHN_V2002 are consistently 3–5 orders
229   of magnitude higher than those observed under H$_2$SO$_4$–H$_2$O binary nucleation conditions without
230   (Fig. 1a) and with (Fig. 1b) the effect of ionizations, while those based on BHN_Y2020 and
231   BIMN_Y2020 are close to the observed values. It should be noted that similar to the CLOUD
232   measurements with the effect of ionization, BHN rates are included in the BIMN rates (Yu et al.,
233   2018) and the difference between BIMN and BHN rates indicates the contribution of ion mediated
234   or induced nucleation. Under the conditions of Fig. 1a, assuming ionization rate of 20 ion-pairs
235   cm^{-3}s^{-1} (within the range of its typical value in the stratosphere) the BIMN rates are about one
236   order of magnitude higher than BHN rates when the nucleation rates are below ~ 5 cm^{-3}s^{-1} but
237   close to BHN rates when nucleation rates are above ~ 5 cm^{-3}s^{-1}. Similar difference between
238   BHN_Y2020 and BIMN_Y2020 can also be seen in Fig. 1b, indicating the importance of ion
239   nucleation at relatively lower nucleation rates (mostly associated with relatively lower [H$_2$SO$_4$])
240   and dominance of homogeneous nucleation at higher nucleation rates (associated with larger
241   [H$_2$SO$_4$]). As we show next, [H$_2$SO$_4$] in the background stratosphere is generally quite low and
242   thus ion nucleation dominates but BHN can become important in the SO$_2$ plumes injected into the
243   stratosphere.

245   **3.2 Nucleation rates and particle number concentrations in the stratosphere**
246   Figure 2 shows the zonal mean SO$_2$ emission (SO$_2$_emit), particle number emitted by aviation
247   (PN_aviation), temperature (T), relative humidity (RH), ionization rate (Q), and [H$_2$SO$_4$] averaged
248   during the two-year period (06/2016–05/2018) covering ATom 1-4. To focus on lower stratosphere
249   (LS), only the values of these variables in the stratosphere (grid boxes with more than 50% time
250   above tropopause) are shown. The SO$_2$ emissions include all sources including volcanos and
251   aviation. During this period, there was one relatively strong volcanic event, the Bezymianny
252   volcano (55.98°N, 160.59°E), on December 20, 2017 that injected 5×10^6 kg S into an altitude of ~
253   14–18 km (Carn et al., 2015). Aviation emission is generally limited to below ~ 12.5 km altitude.
254   Based on MERRA2 meteorology data, which is used to drive GEOS-Chem, almost all of grid
255   boxes at 12 km are under the tropopause in the tropics (30°N-30°S), most of grid boxes at 12 km
256   in the high latitude regions (60°N–90°N, 60°S–90°S) are above tropopause, and some fractions of
257   grid boxes at 12 km in the middle latitude regions (30°N–60°N, 30°S–60°S) are above tropopause.
258   As can be seen from Fig. 2b, some of aviation emissions in the middle and high latitude regions
259   are in the LMS, and the amount emitted into NH LMS is much higher (by several orders of

magnitude) than that in SH. The temperature in the LS ranges from 190–225K, with the lowest value in the region just above tropical tropopause (Fig. 2c). RH in LS has highest values near tropopause but drops quickly with increasing altitude, from ~30–50% near tropopause to ~0.1–1% at ~ 25 km in the tropical and middle latitudes (Fig. 2d). The spatial variations of T and RH have important effects on nucleation in LS. The cosmic ray induced ionization rate in LS has large latitudinal gradient, ranging from ~40–100 ion-pair std. $cm^{-3}s^{-1}$ (here "std. cm^{-3}" refers to per cubic centimeter at standard temperature and pressure, 273 K and 1013 hPa respectively) in the tropics to 100–400 ion-pair std. $cm^{-3}s^{-1}$ in middle and high latitude region (Fig. 2e). The high ionization rates may have important implication for particle microphysics in LS, which will also be discussed in Section 3.3. H_2SO_4 is the most important aerosol precursor in LS and its concentration depends on SO_2 concentrations and oxidation, condensation sink, and its vapor pressure that depends on T and RH. The annual mean $[H_2SO_4]$ (Fig. 2f) has large spatial variations, ranging from a minimum of ~ 1–2 ×10^5 std. cm^{-3} at altitudes of ~ 12–15 km in polar regions to ~ 4–20 ×10^5 std. cm^{-3} close to the tropopause. From ~ 18–25 km (well above the ATom measurement altitude), $[H_2SO_4]$ increases with altitude, mainly due to the increasing H_2SO_4 vapor pressure associated with vertical changes of T (Fig. 2c) and RH (Fig. 2d).
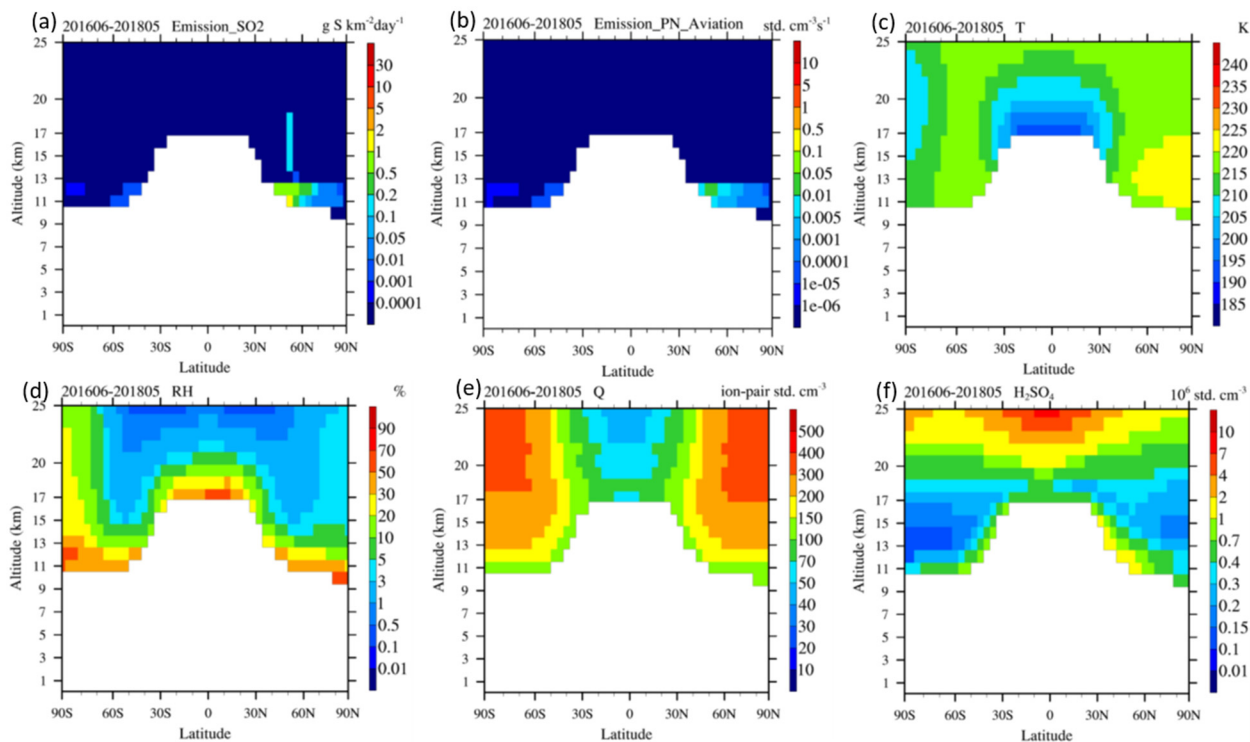
Figure 2. Zonal mean SO_2_emit, PN_Emit, T, RH, Q, and $[H_2SO_4]$ averaged during the two-year period (06/2016-05/2018) covering ATom 1-4. To focus on the lower stratosphere, only the values of these variables in grid boxes with more than 50% time above tropopause and below 25 km are shown.

To demonstrate the effect of nucleation schemes on simulated aerosol properties, we compare in Fig. 3 zonal mean and vertical profiles of nucleation rates (J) and number concentrations of condensation nuclei larger than 3 nm (CN3) simulated based on the three nucleation schemes: BHN_V2002, BHN_Y2020, and BIMN_Y2020. In all three schemes, the aviation emissions of both SO_2 (Fig. 2a) and particle numbers (Fig. 2b) are the same. The model simulations indicate that NPF occurs in the lower stratosphere but is mostly confined to LMS except in the area of volcano injection (for example, above ~ 14 km around ~ 52°N). There exist large differences in the nucleation rates predicted by the three schemes (noting the logarithmic color scale), with BHN_V2002 rates generally 1–4 orders of magnitude higher while BIMN_Y2020 rates ~ one order of magnitude higher than those based on BHN-Y2020. The difference between BIMN_Y2020 and BHN_V2002 rates are smaller in the LMS over tropics (30°S-30°N) where temperature is the lowest (see Fig. 2c). The magnitudes of differences are consistent with comparisons with CLOUD measurements (Fig. 1). The difference in nucleation rates leads to substantial difference in CN3 in LMS, with those based on BHN_V2002 a factor 2–5 higher than those based on BHN_Y2020 in LMS. LMS CN3 based on BIMN_Y2020 is about 50% higher than that of BHN_Y2020. Compared to the difference in nucleation rates, the differences in CN3 is much smaller. This is expected because on one hand only a small fraction of nucleated particles survive the coagulation scavenging and grow beyond 3 nm, and on the other hand direct emission of particle numbers from aviation (Fig. 2b; treated as direct emission but most of these are actually nucleated on chemi-ions in the exhaust plume shortly after emission) (Brock et al., 2000) and transport provide substantial amount of CN3 even without nucleation. Nevertheless, nucleation is still significant enough to affect the CN3. It is interesting to note that CN3 based on BIMN_Y2020 is higher at altitudes > ~ 22 km (Fig. 3h), which is associated with higher nucleation rates based on BIMN_Y2020 than those based on BHN_V2002 and BHN_Y2020 within the altitude range of 35-55 km. Another interesting point is that there is a much smaller vertical gradient in BHN_V2002 nucleation rates in the tropical region (30S-30N) within ~ 17-20 km (see Figs. 3a and 3d), likely a result of different dependences of nucleation rates based on different schemes on T, RH, and [H_2SO_4] which have large vertical variations (see Fig. 2). It can be seen from Fig. 3 that the simulations based on three nucleation schemes all show large hemispheric difference in particle number concentrations (by a factor of ~3-6) in LMS at middle and high latitudes, consistent with the ATom measurements (Williamson et al., 2021). Our sensitivity study (by turning off aviation emission, not shown, to be reported in a separate study) indicates this large hemispheric difference is largely caused by aviation emissions, confirming the analysis of Williamson et al. (2021).
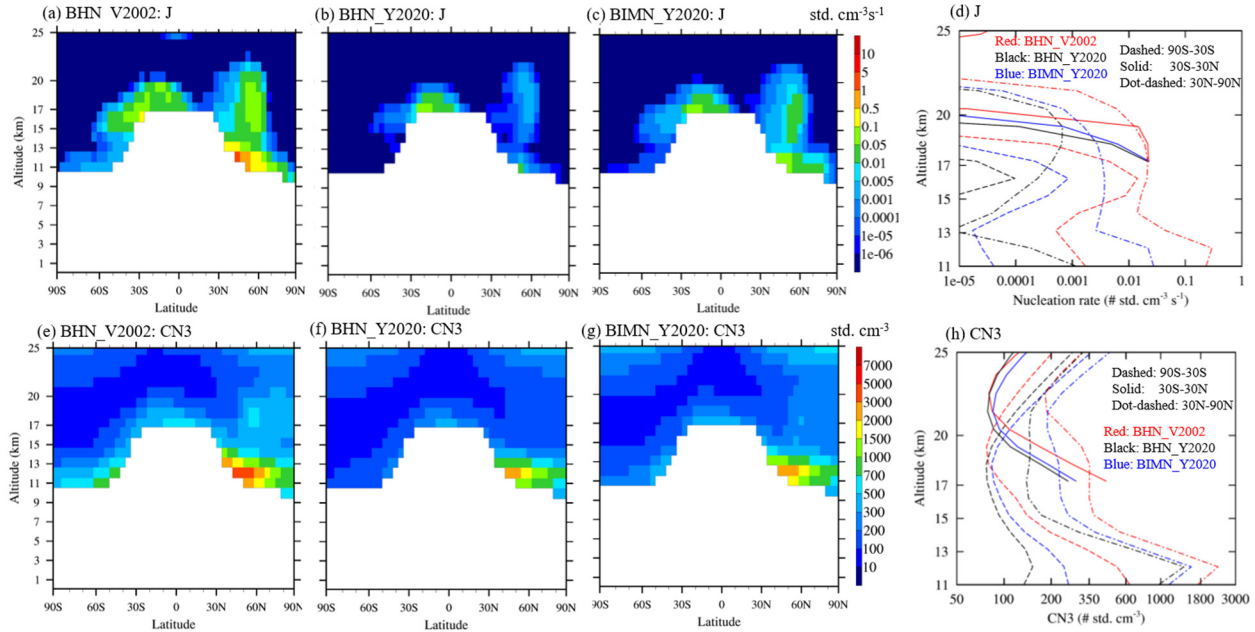
Figure 3. Model simulated zonal mean and vertical profiles of nucleation rates (J; upper panels) and number concentrations of particles larger than 3 nm (CN3; lower panels) in the stratosphere during the two-year period covering ATom 1-4 (06/2016- 05/2018), based on three nucleation schemes (a&e: BHN_V2002, b&f: BHN_Y2020, and c&g: BIMN_Y2020). The vertical profiles in (d) and (h) are averaged for three latitude zones (90S-30S, 30S-30N, and 30N-90N). The values for those grids with at least 50% of time above the tropopause are shown.

While it is difficult to observe nucleation rates in the stratosphere, the measurement of freshly nucleated nanoparticles can be used to constrain nucleation schemes. Figure 4a compares the model simulated CN3 (all particles with diameter larger than 3 nm, with the upper size limit of 12 μm corresponding to the size of last model bin) based on the three nucleation schemes at altitudes of around 12 km in SH middle and high altitudes during four seasons with the corresponding ATom 1–4 observations. As an example, Figures 4b–d show the model simulated horizontal distributions of CN3 at 12 km altitude during ATom 4 with the values and locations of ATom4 CN3 data overlaid. We choose SH for comparison, as it represents the background stratosphere with minimum influence of anthropogenic emissions (i.e., aviation) (Fig. 2b), to avoid the uncertainty associated with aviation emissions. In Figure 4, the model results are two-month average corresponding to the flight months of each ATom campaign while the measurement data points shown are those sampled within the altitudes range of 11.5–12.5 km, in the stratosphere (ozone>250 ppbv and RH<10%, following the same stratosphere definitions as in Murphy et al. (2021) and Williamson et al. (2021)), and averaged to a 4°x5° gridbox for comparison with modeled results. The impact of nucleation scheme on CN3 can be clearly seen: BHN_V2002 overpredicted CN3 by a factor of 2–4, BHN_Y2020 slightly underpredicted CN3, and BIMN_Y2020 slightly overpredicted CN3. The larger vertical spread in CN3 from BHN_V2002 is caused by the large CN3 latitude gradient associated with higher nucleation near tropopause

345 (Fig. 3). The comparisons above show that the ATom measurements provide a good constraint on
346 our understanding of the processes controlling CN3 in the LMS at mid-high latitudes.
347
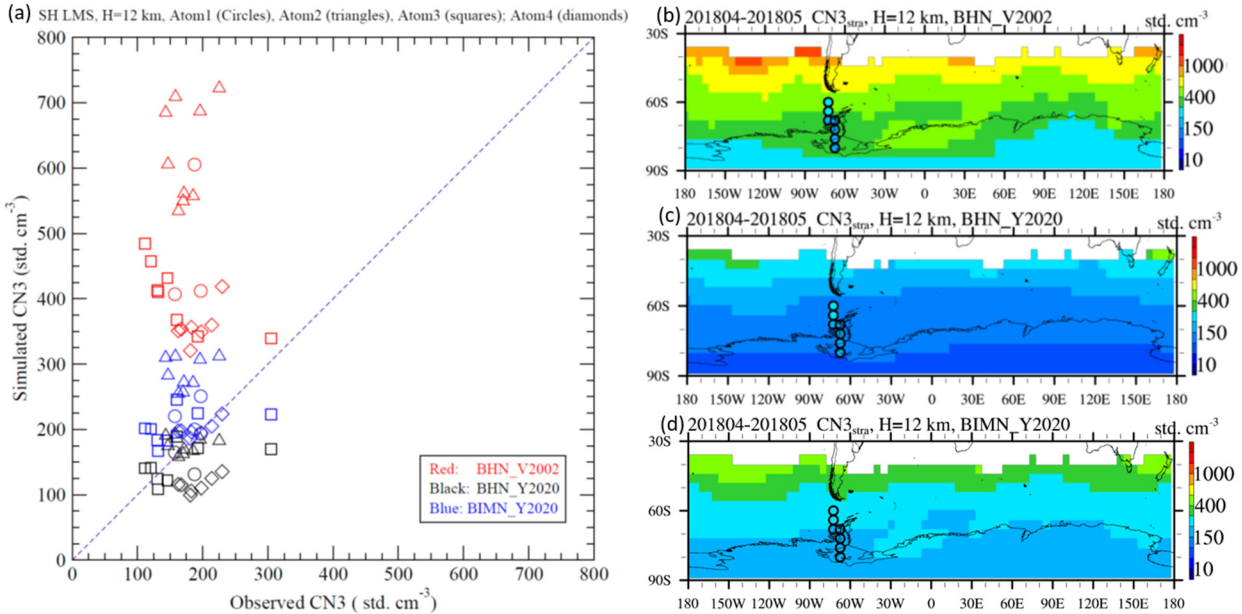
349 **Figure 4.** CN3 at altitudes of around 12 km in SH middle and high latitudes: (a) Model simulated
350 versus observed during ATom 1-4 (Circles: ATom1; Triangles: ATom2; Sqaures: ATom3;
351 Diamonds: ATom4); (b-d) model simulated horizontal distributions corresponding to ATom 4
352 based on three different nucleation schemes (BHN_V2002, BHN_Y2020, and BIMN_Y2020),
353 with the values and locations of ATom 4 CN3 measurements shown in the circles.

354

355 **3.3 PNSDs in the stratosphere**

356 Figure 5 shows the model simulated evolution of PNSDs at an altitude of 12 km over a site in
357 SH (70°S, 60°W) during the two-year ATom period based on the three different nucleation
358 schemes. The PNSDs shown in Fig. 5 are averaged into four different seasons corresponding to
359 the months of ATom 1-4 field campaigns and are presented in Fig. 6 for comparison with the
360 observed mean PNSDs in SH LMS (Williamsons et al., 2021). It should be noted that modeled
361 PNSDs in Fig. 6 are two-month average at one fixed site at an altitude of 12 km (in the region
362 where many of SH LMS measurements were taken, see Fig. 4) while the observed ones are
363 averaged over all SH LMS air mass sampled during the corresponding ATom campaign. While
364 the comparison in Fig. 6 is not exactly coterminous, it allows us to make quantitative comparisons
365 of modeled and observed PNSDs. To take into account the variations in both model and observed
366 PNSDs, standard deviations are shown as error bars in the measured and modeled curves based on
367 BIMN_Y2020.

368
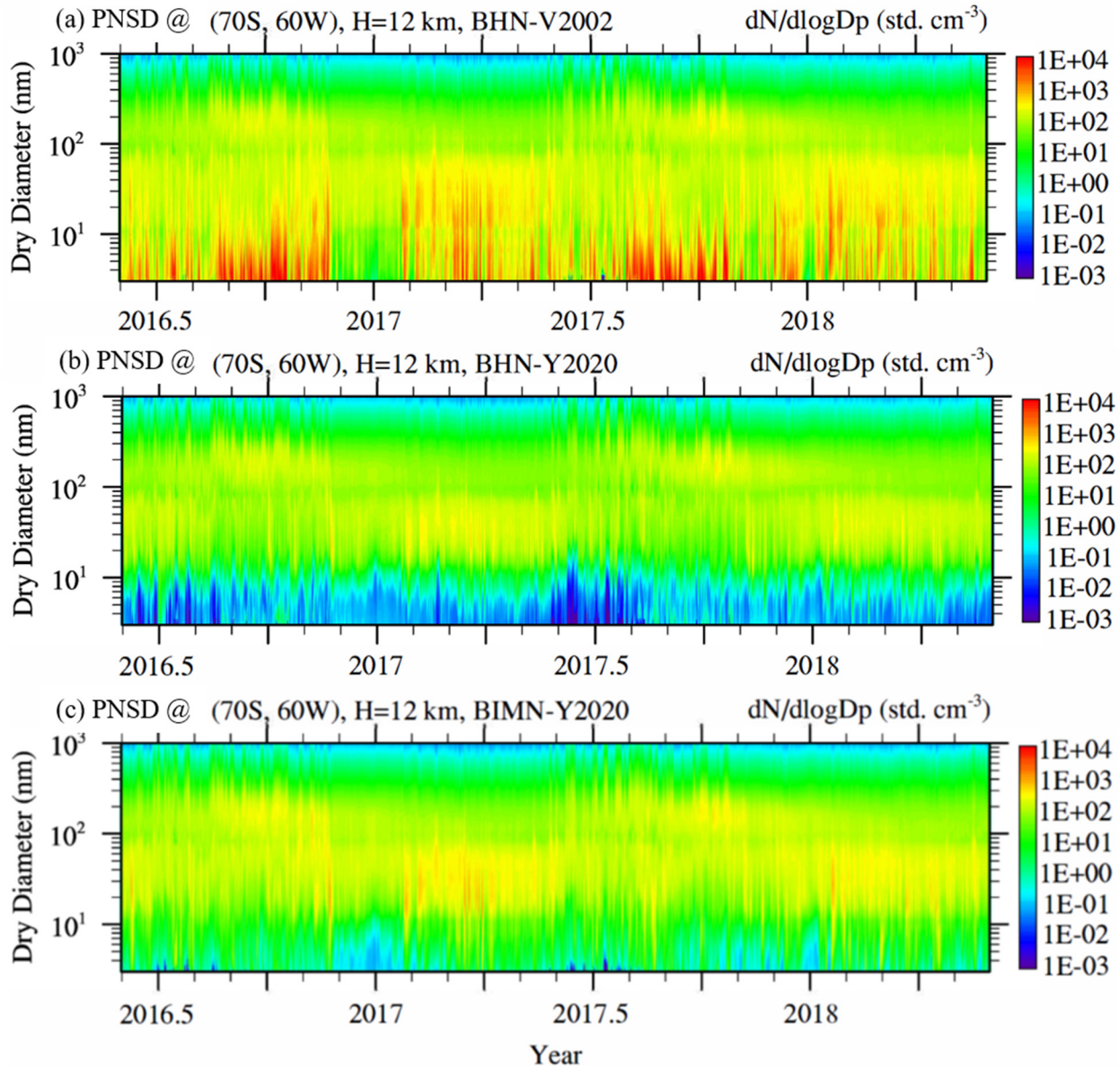
Figure 5. Model simulated evolution of PNSDs at a site in SH (70S, 60 W) at altitude of 12 km based on three nucleation schemes (BHN_2002, BHN_Y2020, and BIMN_Y2020).

Figure 6 shows that PNSDs measured in the background LMS have multiple modes: a nucleation mode (NuclM: $\lesssim$ 10 nm), an Aitken mode (AitkenM: ~10 – 80 nm), and two accumulation modes (AccuM1: ~ 80 – 250 nm and AccuM2: ~ 250 – 700 nm). It should be noted that these modes are not the same size limits as those presented in the public ATom dataset. As shown in Figures 5 and 6, the model based on all three nucleation schemes generally captures the AitkenM and AccuM1 and the existence of a minimum in PNSDs around 80 nm, although there exist differences. Interestingly, the relative height (or peak values of dN/dlogD$_p$) of AitkenM and AccuM1 has strong seasonal variations. The model captures a relatively higher AitkenM in SH Summer and Fall and a higher AccuM1 in SH Spring. The model simulated PNSDs also agree

382 well with the measurements in term of the size-dependent normalized standard deviation (σ_N, i.e.,
383 the standard deviation σ divided by the mean): relatively smaller σ_N for AccuM1 and larger size
384 part of AitkenM and much larger σ_N for NuclM, smaller size part of AitkenM, and AccuM2. While
385 the larger σ_N for NuclM is understandable because of NPF, it is surprising for AccuM2. The
386 AccuM2 particles have relatively long lifetime and are expected to be well-mixed (and thus have
387 small variations) in LS. The transport of AccuM2 particles from UT may contribute to the larger
388 variations. Murphy et al. (2021) showed the chemical signature of this transported mode, and here
389 we show that the variation in the size distribution may also contain information about the mixing
390 of UT particles into LMS. Compared to the observations, the model simulated AccuM2 σ_N are
391 larger in SH Winter and Spring but are smaller in SH Summer and Fall. The possible reasons for
392 the large variations of AccuM2 in LMS and the differences between model simulations and
393 measurements remain to be studied.
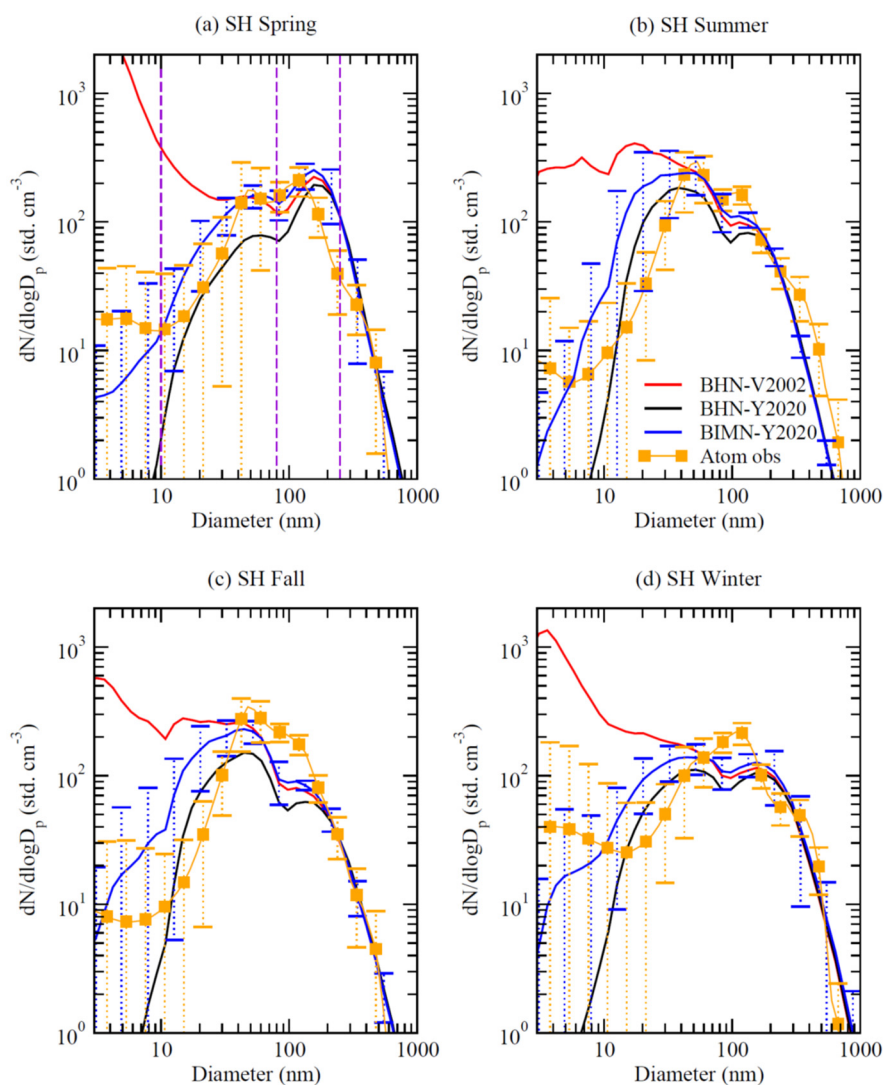
394
395 **Figure 6.** Model simulated seasonal mean PNSDs at a site in SH (70°S, 60°W) at altitude of 12
396 km based on three nucleation schemes and comparisons with the corresponding ATom
397 measurements (a: SH Spring 09–10/2017, b: SH Summer 01–02/2017, c: SH Fall 04–05/2018, and

398 d: SH Winter 06–07/2016). To take into account the variations in both model and observed PNSDs,
399 standard deviations are shown as error bars in the measured and modeled curves based on
400 BIMN_Y2020. Three vertical dashed lines at 10 nm, 80 nm, and 250 nm are drawn in (a) to guide
401 the eye to the four modes discussed in the text.

402
403

404 The large impacts of nucleation schemes on PNSDs, especially those smaller than 100 nm, can
405 be seen in Fig. 6. The formation rates and concentrations of nucleation mode particles are very
406 high based on BHN_V2002 (peak dNdlogDp values reaching well above 10^3 std. cm^{-3}), negligible
407 based on BHN_Y2020 (dNdlogDp values for particles <10 nm are generally below 1 std. cm^{-3}),
408 and moderate based on BIMN_Y2020. When compared to the observed values, the number
409 concentrations of particles within 3–10 nm based on BHN_V2002 are 1–2 orders of magnitude
410 too high but those based on BHN_Y2020 are 1–2 orders of magnitudes too low, while those based
411 on BIMN_Y2020 are of the same order of magnitude. The impact of nucleation schemes on NuclM
412 propagates into the AitkenM and AccuM1, with BHN_Y2020 giving the lowest number
413 concentrations while BHN_V2002 gives the highest AitkenM and BIMN_Y2020 gives the highest
414 AccuM1. It should be noted that, while the line of BHN-Y2020 is lower than that of BIMN and
415 BHN-V2002 for particles of smaller sizes (<~ 300 nm), it is slightly higher for larger particles (>~
416 300 nm). This is consistent with the competition of sulfuric acid gas between pre-existing larger
417 particles and nucleated smaller particles. It is interesting to note that AccuM1 based on
418 BIMN_Y2020 is higher than that based on BHN_V2002 although BHN_V2002 predicts higher
419 NuclM and AitkenM, indicating a non-linear interaction among nucleation, growth, and
420 coagulation. The competition between nucleation and condensation for available sulfuric acid gas
421 has been shown to be important for SAI studies (Laakso et al., 2022).
422 There exist a number of differences in the simulated and observed PNSDs. Firstly,
423 measurements indicate a slight increase of dNdlogD$_p$ with decreasing sizes for particles < 10 nm
424 but the simulated PNSDs based on BIMN_Y2020, the scheme mostly consistent with CLOUD
425 measurements and predicting NuclM concentrations closest to those observed, decreases with
426 decreasing sizes for particles < 10 nm. The possible reasons of the difference remain to be
427 investigated but probably are associated with uncertainty in nucleation rates and size-dependent
428 growth rates of freshly nucleated particles, and/or the fact that ATom observations are bias towards
429 daytime. In addition, the small number of particles in this mode is likely within the uncertainty in
430 the ATom measurements (about 7% of the total number of particles), so that this measured mode
431 may not be significant. Secondly, the model appears to overpredict the smaller size part (~10–40
432 nm) of AitkenM although it is close to the larger part of the mode (~40–80 nm). The overprediction
433 may be a result of the underestimated growth rates or coagulation scavenging rates of these
434 particles or overpredicted growth rates of NuclM particles. Thirdly, the model generally
435 overpredicts the mean mode sizes of AccuM1 and underpredicts the concentrations of the mode
436 except in SH Spring. The nucleation schemes have observable effects on the concentrations and
437 mean sizes of AccuM1 and overall the simulations based on BIMN_Y2020 are in stronger
438 agreement with measurements. Finally, the observed PNSDs show a clear AccuM2 in all seasons
439 except Fall but such a mode cannot be clearly seen in the model simulated PNSDs, indicating that
440 the model underpredicts the concentrations of AccuM2 mode particles. AccuM2 particles are

within the size range with most efficient scattering of solar radiation and thus are important for SAI. It is therefore necessary to identify the sources of this difference and to improve the model.

As pointed out earlier, the comparison in Fig. 6 does not exactly match in terms of time and location, which likely contributes to some of the differences shown in Fig. 6. Some of the differences can also be caused by the uncertainties in the model in term of emissions, transport, chemistry, aerosol microphysics, and deposition. Nevertheless, some of these differences, especially the shape of PNSDs (AccuM2, NuclM, etc.), are unlikely to be fully accounted for by the above-mentioned possible mismatch or model uncertainties and thus may indicate that some fundamental processes are not represented in the model. One possible cause of the differences is that the transport of organic-sulfate particles from UT (Murphy et al., 2014, 2021) is not properly simulated by the model. Based on size-resolved particle composition measurements, Murphy et al. (2021) showed that the LMS accumulation mode particles (diameter ~ 0.1 and 1.0 μm) have at least two modes: the larger mode consists mostly of sulfuric acid particles produced in the stratosphere, and the smaller mode consists mostly of organic-sulfate particles transported from the troposphere. Murphy et al. (2014) showed that the fraction of organic-sulfate aerosols above tropopause decreases quickly with altitudes. While the organic-sulfate mode aerosols from UT may contribute to the bi-modal structure of accumulation mode particles in the LMS observed during ATom, it is unlikely to contribute to the bi-modal structure of particles larger than ~200 nm observed at altitude above ~20 km both in the background and in volcano perturbed stratosphere (Deshler et al., 2013, 2019; also see Fig. 7). Here, we suggest that the role of charges on coagulation and growth of particles in the stratosphere could be another process causing the bi-modal of large particles in the stratosphere.

As shown Fig. 2e, ionization rates are high in LS, ranging from ~ 40–100 ion-pair std. $cm^{-3}s^{-1}$. Due to their low number concentrations (~100–1000 std. cm^{-3}) but long lifetime, particles in the stratosphere are expected to be in charge equilibrium. Figure 7 shows mean particle number size distribution (PNSD) and particle volume size distribution (PVSD) observed during ATom 1-4 in SH LMS and measured within 20-25 km altitude over Lararie WY in 1992, and fraction of particles carrying n charges based on the modified Boltzmann equilibrium equation (Clement and Harrison, 1992). The bi-modal structure of accumulation mode particles can be clearly seen in both background and volcano perturbed stratosphere. It should be noted that while the smaller mode generally dominates the number concentrations, the larger mode dominates mass concentrations. Under equilibrium more particles are charged (i.e., $1-f_0 > 50\%$) than neutral (f_0) for particles with diameter larger than ~80 nm and a significant fraction (> 25%) of particles larger than 300 nm carrying multiple charges. While the equilibrium charge fraction is small for NuclM particles ($\lesssim$ 10 nm), this fraction can be much larger when nucleation on ions occurs, which is consistent with the observed overcharging of freshly nucleated particles (Laakso et al. 2007; Yu and Turco, 2008). Particle coagulation rates are influenced by forces exerted between colliding particles, including van der Waals and electrostatic forces, which can modify the effective collision cross section and sticking coefficient. The van der Waals force has been shown to be important in the stratosphere (English et al., 2011, 2012) and has been considered in the simulations shown above. The effects of charges on coagulation and implications for PNSDs in the stratosphere have not yet been studied (to our knowledge). Since coagulation is a dominant process for the growth of accumulation mode particles in the stratosphere, we hypothesize that differential coagulation rates for neutral and

484 charged particles in accumulation modes can potentially act as a physical process separating the
485 modeled single accumulation mode (Fig. 6) into two modes (AccuM1 and AccuM2) as observed.
486 Further research is needed to test this hypothesis. In addition to affecting coagulation, charge on
487 small particles can also enhance the growth rate due to ion-dipole interactions of condensing
488 molecules with charged particles (Nadykto and Yu, 2005). This enhancement is expected to be
489 stronger in the stratosphere because of lower temperature (Nadykto and Yu, 2005). Beside these,
490 Svensmark et al. (2020) showed that the condensation of ion clusters can enhance particle growth
491 rates. How much the enhanced coagulation and growth rates of charged particles may shape
492 PNSDs and modes in the stratosphere remains to be investigated.
493
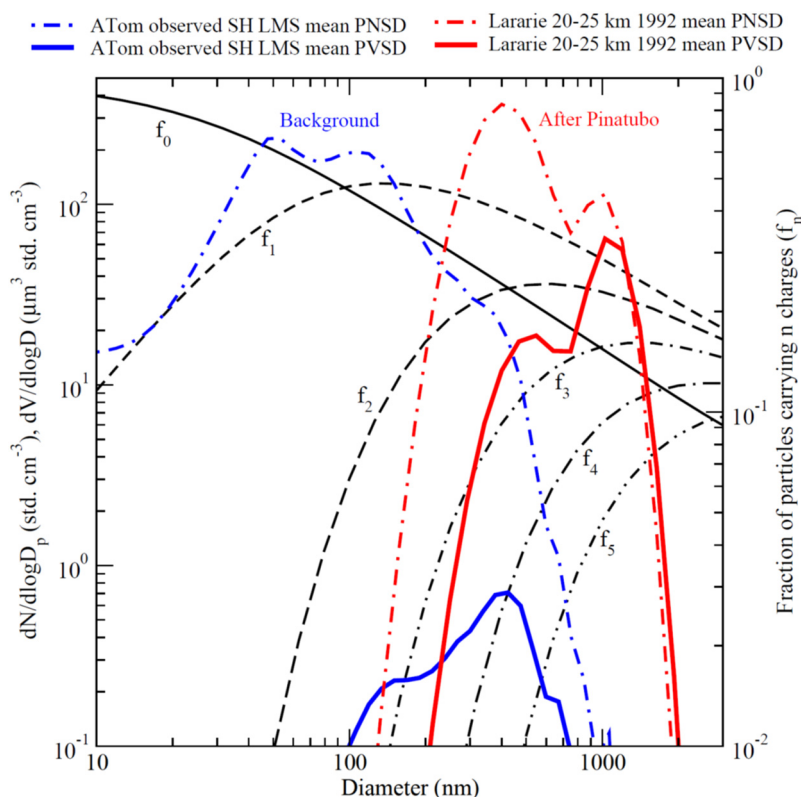
494
495 **Figure 7.** ATom 1-4 mean observed particle number size distribution (PNSD, or dN/dlogDp) and
496 particle volume size distribution (PVSD, or dV/dlogDp) in SH LMS, balloon-borne measured
497 mean PNSD and PVSD within 20-25 km altitude over Lararie WY in 1992, and fraction of
498 particles carrying n ($n = 0, 1, 2, 3, 4,$ and 5) charges based on the modified Boltzmann equilibrium
499 equation (Clement and Harrison, 1992). Note that f_n with $n \geq 1$ including both positive and negative
500 charges, i.e., for example, half of f_1 carrying one negative charge while the other half positive.
501

4. Summary and Discussions

503   Interest in stratospheric aerosols has been increasing in recent years, due to the ongoing
504 discussion about the plausibility, potential benefits and risks of offsetting climate change through
505 stratospheric aerosol injection (SAI) to buy time for reduction of CO_2 in the atmosphere. Recent
506 studies indicate the dependence of SAI radiative efficacy (Dai et al., 2018) on the particle size
507 distribution (NASEM, 2021) and thus it is critical to improve foundational understanding and

model representation of aerosol microphysics processes controlling the evolution of stratospheric aerosols, both under background conditions and perturbed scenarios. While formation and growth of particles in the troposphere have been extensively studied in the past two decades, very limited efforts have been devoted to understanding these in the stratosphere.

In the present study we use both CLOUD laboratory measurements taken under very low stratospheric temperatures and ATom in-situ observations of particle number size distributions (PNSD) down to 3 nm to constrain nucleation schemes and model-simulated particle size distributions in the lowermost stratosphere (LMS). We show that the binary homogenous nucleation scheme used in most of the existing SAI modeling studies overpredicts the nucleation rates by 3–4 orders of magnitude (when compared to CLOUD data), leading to significant overprediction of particle number concentrations in the background stratosphere (by a factor of 2–4 in SH LMS, compared to ATom data). Based on a recently developed kinetic nucleation model which provides rates of both ion-mediated nucleation (IMN) and BHN at low temperatures in good agreement with CLOUD measurements, both BHN and IMN occur in the stratosphere but IMN rates are generally more than one order of magnitude higher than BHN rates and thus dominate nucleation in the background stratosphere.

In the SH LMS that has minimal influences from anthropogenic emissions, our analysis shows that ATom-measured PNSDs generally have four apparent modes: a nucleation mode (NuclM: $\lesssim$ 10 nm), which may not be statistically significant, an Aitken mode (AitkenM: ~10–80 nm), and two accumulation modes (AccuM1: ~ 80–250 nm and AccuM2: ~ 250–700 nm). The model generally captures the AitkenM and AccuM1 and the existence of a minimum in PNSDs at ~ 80 nm, although there are differences. The model captures a relatively higher AitkenM in SH Summer and Fall and a higher AccuM1 in SH Spring. The model simulated PNSDs also agree well with the measurements in term of the size-dependent standard deviations: relatively smaller standard deviations for AccuM1 and larger size part of AitkenM and much larger standard deviations for NuclM, smaller size part of AitkenM, and AccuM2.

A detailed comparison indicates the existence of a third PNSD mode peaking around 300–400 nm in the ATom measurements that are not captured by the model. Compared to the observations, the model-simulated AccuM2 standard deviations are larger in SH Winter and Spring but are smaller in SH Summer and Fall. In addition, the model overpredicts the number concentration of particles in the size range of 10–50 nm. These differences may indicate that, in addition to nucleation, the model may be missing some fundamental microphysical processes of stratospheric aerosols. Our analysis shows that, in the stratosphere, more particles are charged (positive + negative) than neutral for particles with diameter larger than ~80 nm and a significant fraction (> 25%) of particles larger than 300 nm carrying multiple charges. We propose that the role of charges on coagulation and growth of particles in the stratosphere, where ionization rates are high and particles have very long lifetime, is likely one of such processes. Considering the importance of accurate particle size distributions (especially the accumulation mode particles) for projecting realistic radiative forcing response to stratospheric aerosols, it is essential to understand and incorporate such potentially important processes in model simulations of future changes in the stratosphere. It should be noted that the ATom measurement period does not have a high stratospheric aerosol loading (i.e., no major volcano eruptions). It remains to be investigated if previous assessments of volcanic aerosol microphysics missed something important. We expect

the uncertainties in the nucleation schemes and unknown cause of the bi-modal structure of accumulation mode particles will affect particle optical properties and surface area and thus radiative forcing or chemistry. In addition to what we have shown in this study, there are likely other uncertainties or missing processes we do not know and the community needs to identify and resolve these. The present work highlights the importance of advancing scientific understanding of processes controlling properties of stratospheric particles, identifying important processes that the present models might have missed, and further development, improvement, and validation of models for reducing uncertainties of SAI simulations (e.g., Golja et al., 2021, Sun et al., 2022).

Conflict of interest: The authors declare that they have no conflict of interest.

Acknowledgments. The MERRA-2 data used in this study have been provided by the Global Modeling and Assimilation Office (GMAO) at NASA Goddard Space Flight Center. This research has been supported by NASA (grant nos. 80NSSC19K1275 and 80NSSC21K1199) and SilverLining.

Data availability. The GEOS-Chem model is available to the public at https://geos-chem.seas.harvard.edu/. Simulation output in this analysis is available at https://doi.org/10.5281/zenodo.6909944. The ATom dataset is published as Wofsy et al., (2021, https://doi.org/10.3334/ORNLDAAC/1925) and is also available at https://espoarchive.nasa.gov/archive/browse/atom (last access: June 2022).

References

Brock, C. A., Hamill, P., Wilson, J. C., Jonsson, H. H., and Chan, K. R.: Particle formation in the upper tropical troposphere – A source of nuclei for the stratospheric aerosol, Science, 270, 1650–1653, https://doi.org/10.1126/science.270.5242.1650, 1995.

Brock, C. A., Schröder, F., Kärcher, B., Petzold, A., Busen, R., and Fiebig, M.: Ultrafine particle size distributions measured in aircraft exhaust plumes, J. Geophys. Res.-Atmos., 105, 26555–26567, https://doi.org/10.1029/2000jd900360, 2000.

Brock, C. A., Williamson, C., Kupc, A., Froyd, K. D., Erdesz, F., Wagner, N., Richardson, M., Schwarz, J. P., Gao, R.-S., Katich, J. M., Campuzano-Jost, P., Nault, B. A., Schroder, J. C., Jimenez, J. L., Weinzierl, B., Dollner, M., Bui, T., and Murphy, D. M.: Aerosol size distributions during the Atmospheric Tomography Mission (ATom): methods, uncertainties, and data products, Atmos. Meas. Tech., 12, 3081–3099, https://doi.org/10.5194/amt-12-3081-2019, 2019.

Brock, C.A., Froyd, K.D., Dollner, M., Williamson, C.J., Schill, G., Murphy, D.M., Wagner, N.J., Kupc, A., Jimenez, J.L., Campuzano-Jost, P., Nault, B.A., Schroder, J.C., Day, D.A., Price, D.J., Weinzierl, B., Schwarz, J.P., Katich, J.M., Wang, S., Zeng, L., Weber, R., Dibb, J., Scheuer, E., Diskin, G.S., DiGangi, J.P., Bui, T., Dean-Day, J.M., Thompson, C.R., Peischl, J., Ryerson, T.B., Bourgeois, I., Daube, B.C., Commane, R., and Wofsy, S.C. Ambient aerosol properties in the remote atmosphere from global-scale in situ measurements, Atmos. Chem. Phys., 21: 15023-63. 2021.

Carn, S. A., Yang, K., Prata, A. J. and Krotkov, N. A.: Extending the long-term record of volcanic SO2 emissions with the Ozone Mapping and Profiler Suite nadir mapper. Geophys. Res. Lett., 42: 925– 932. doi: 10.1002/2014GL062437, 2015.

Clement, C. F., & Harrison, R. G.: The charging of radioactive aerosols. Journal of Aerosol Science, 23(5), 481–504. https://doi.org/10.1016/0021-8502(92)90019-R, 1992.

Dai, Z., Weisenstein, D. K., & Keith, D. W.: Tailoring meridional andseasonal radiative forcing by sulfateaerosol solar geoengineering.Geophysical Research Letters,45,1030–1039. https://doi.org/10.1002/2017GL076472, 2018.

Dawson, M. L., Varner, M. E., Perraud, V., Ezell, M. J., Gerber, R. B., & Finlayson-Pitts, B. J.: Simplified mechanism for new particle formation from methanesulfonic acid, amines, and water via experiments and ab initio calculations. Proceedings of the National Academy of Sciences, 109(46), 18719-18724, 2012.

Dunne, E. M., Gordon, H., Kürten, A., Almeida, J., Duplissy, J., Williamson, C., Ortega, I. K., Pringle, K. J., Adamov, A., Baltensperger, U., Barmet, P., Benduhn, F., Bianchi, F., Breitenlechner, M., Clarke, A., Curtius, J., Dommen, J., Donahue, N. M., Ehrhart, S., Flagan, R. C., Franchin, A., Guida, R., Hakala, J., Hansel, A., Heinritzi, M., Jokinen, T., Kangasluoma, J., Kirkby, J., Kulmala, M., Kupc, A., Lawler, M. J., Lehtipalo, K., Makhmutov, V., Mann, G., Mathot, S., Merikanto, J., Miettinen, P., Nenes, A., Onnela, A., Rap, A., Reddington, C. L. S., Riccobono, F., Richards, N. A. D., Rissanen, M. P., Rondo, L., Sarnela, N., Schobesberger, S., Sengupta, K., Simon, M., Sipilä, M., Smith, J. N., Stozkhov, Y., Tomé, A., Tröstl, J., Wagner, P. E., Wimmer, D., Winkler, P. M., Worsnop, D. R., and Carslaw, K. S.: Global particle formation from CERN CLOUD measurements, Science, 354, 1119–1124, https://doi.org/10.1126/science.aaf2649, 2016.

Eastham, S. D., Weisenstein, D. K., & Barrett, S. R.: Development and evaluation of the unified tropospheric–stratospheric chemistry extension (UCX) for the global chemistry-transport model GEOS-Chem. Atmospheric Environment, 89, 52-63, 2014.

English, J. M., Toon, O. B., Mills, M. J., & Yu, F.: Microphysical simulations of new particle formation in the upper troposphere and lower stratosphere. Atmospheric Chemistry and Physics, 11(17), 9303-9322, 2011.

Evans, M. J., & Jacob, D. J.: Impact of new laboratory studies of N2O5 hydrolysis on global model budgets of tropospheric nitrogen oxides, ozone, and OH. Geophysical Research Letters, 32(9), 2005.

Golja, C. M., Chew, L. W., Dykema, J. A., & Keith, D. W.: Aerosol dynamics in the near field of the SCoPEx stratospheric balloon experiment. Journal of Geophysical Research: Atmospheres, 126, e2020JD033438. https://doi. org/10.1029/2020JD033438, 2021.

Gronoff, G., Berkoff, T., Knowland, K. E., Lei, L., Shook, M., Fabbri, B., Carrion, W., & Langford, A. O.: Case study of stratospheric Intrusion above Hampton, Virginia: lidar-observation and modeling analysis. Atmospheric Environment, 118498, 2021.

Hamill, P., Turco, R. P., Kiang, C. S., Toon, O. B., and Whitten, R. C.: An analysis of various nucleation mechanisms for sulfate particles in the stratosphere, J. Aerosol Sci., 13, 561–585, 1982.

Hoesly, R. M., Smith, S. J., Feng, L., Klimont, Z., Janssens-Maenhout, G., Pitkanen, T., Seibert, J. J., Vu, L., Andres, R. J., Bolt, R. M., Bond, T. C., Dawidowski, L., Kholod, N., Kurokawa,

J.-I., Li, M., Liu, L., Lu, Z., Moura, M. C. P., O'Rourke, P. R., and Zhang, Q.: Historical (17502014) anthropogenic emissions of reactive gases and aerosols from the Community Emissions Data System (CEDS), Geosci. Model Dev., 11, 369-408, 2018.

Holmes, C. D., Bertram, T. H., Confer, K. L., Graham, K. A., Ronan, A. C., Wirks, C. K., & Shah, V.: The role of clouds in the tropospheric NOx cycle: A new modeling approach for cloud chemistry and its global implications. Geophysical Research Letters, 46(9), 4980-4990, 2019.

IPCC. Climate Change 2021: The Physical Science Basis. Contribution of Working Group I to the Sixth Assessment Report of the Intergovernmental Panel on Climate Change [Masson-Delmotte, V., P. Zhai, A. Pirani, S. L. Connors, C. Péan, S. Berger, N. Caud, Y. Chen, L. Goldfarb, M. I. Gomis, M. Huang, K. Leitzell, E. Lonnoy, J. B. R. Matthews, T. K. Maycock, T. Waterfield, O. Yelekçi, R. Yu and B. Zhou (eds.)]. Cambridge University Press, 2021.

Jones, A., Haywood, J. M., Jones, A. C., Tilmes, S., Kravitz, B., and Robock, A.: North Atlantic Oscillation response in GeoMIP experiments G6solar and G6sulfur: why detailed modelling is needed for understanding regional implications of solar radiation management, Atmos. Chem. Phys., 21, 1287–1304, https://doi.org/10.5194/acp-21-1287-2021, 2021.

Kärcher, B., Turco, R. P., Yu, F., Danilin, M. Y., Weisenstein, D. K., Miake-Lye, R. C., & Busen, R.: A unified model for ultrafine aircraft particle emissions. Journal of Geophysical Research: Atmospheres, 105(D24), 29379-29386, 2000.

Keller, C. A., Long, M. S., Yantosca, R. M., Da Silva, A. M., Pawson, S., and Jacob D. J.: HEMCO v1.0: a versatile, ESMF-compliant component for calculating emissions in atmospheric models, Geosci. Model Dev., 7, 1409–1417, 2014.

Kerminen, V. M., Chen, X., Vakkari, V., Petäjä, T., Kulmala, M., & Bianchi, F.: Atmospheric new particle formation and growth: review of field observations. Environmental Research Letters, 13(10), 103003, 2018.

Kirkby, J., Curtius, J., Almeida, J., Dunne, E., Duplissy, J., Ehrhart, S., Franchin, A., Gagné, S., Ickes, L., Kürten, A., Kupc, A., Metzger, A., Riccobono, F., Rondo, L., Schobesberger, S., Tsagkogeorgas, G., Wimmer, D., Amorim, A., Bianchi, F., Breitenlechner, M., David, A., Dommen, J., Downard, A., Ehn, M., Flagan, R. C., Haider, S., Hansel, A., Hauser, D., Jud, W., Junninen, H., Kreissl, F., Kvashin, A., Laaksonen, A., Lehtipalo, K., Lima, J., Lovejoy, E. R., Makhmutov, V., Mathot, S., Mikkilä, J., Minginette, P., Mogo, S., Nieminen, T., Onnela, A., Pereira, P., Petäjä, T., Schnitzhofer, R., Seinfeld, J. H., Sipilä, M., Stozhkov, Y., Stratmann, F., Tomé, A., Vanhanen, J., Viisanen, Y., Vrtala, A., Wagner, P. E., Walther, H., Weingartner, E., Wex, H., Winkler, P. M., Carslaw, K. S., Worsnop, D. R., Baltensperger, U., and Kulmala, M.: The role of sulfuric acid, ammonia and galactic cosmic rays in atmospheric aerosol nucleation, Nature, 476, 429–433, 2011.

Kirner, O., Ruhnke, R., Buchholz-Dietsch, J., Jöckel, P., Brühl, C., & Steil, B.: Simulation of polar stratospheric clouds in the chemistry-climate-model EMAC via the submodel PSC. Geoscientific Model Development, 4(1), 169-182, 2011.

Knowland, K. E., Keller, C. A., Wales, P. A., Wargan, K., Coy, L., Johnson, M. S., et al. (2022). NASA GEOS Composition Forecast Modeling System GEOS-CF v1.0: Stratospheric composition. Journal of Advances in Modeling Earth Systems, 14, e2021MS002852. https://doi.org/10.1029/2021MS002852.

Kravitz, B., Robock, A., Boucher, O., Schmidt, H., Taylor, K. E., Stenchikov, G., & Schulz, M.: The geoengineering model intercomparison project (GeoMIP). Atmospheric Science Letters, 12(2), 162-167, 2011.

Kulmala, M., Vehkamäki, H., Petäjä, T., Dal Maso, M., Lauri, A., Kerminen, V. M., W. Birmili, & McMurry, P. H.: Formation and growth rates of ultrafine atmospheric particles: a review of observations. Journal of Aerosol Science, 35(2), 143-176. doi: 10.1016/j.jaerosci.2003.10.003, 2004.

Kupc, A., Williamson, C., Wagner, N. L., Richardson, M., & Brock, C. A.: Modification, calibration, and performance of the Ultra-High Sensitivity Aerosol Spectrometer for particle size distribution and volatility measurements during the Atmospheric Tomography Mission (ATom) airborne campaign. Atmospheric Measurement Techniques, 11(1), 369-383. doi:10.5194/amt-11-369-2018, 2018.

Kupc, A., Williamson, C. J., Hodshire, A. L., Kazil, J., Ray, E., Bui, T. P., Dollner, M., Froyd, K. D., McKain, K., Rollins, A., Schill, G. P., Thames, A., Weinzierl, B. B., Pierce, J. R., and Brock, C. A.: The potential role of organics in new particle formation and initial growth in the remote tropical upper troposphere, Atmos. Chem. Phys., 20, 15037-15060, 10.5194/acp-20-15037-2020, 2020.

Kürten, A., Bianchi, F., Almeida, J., Kupiainen-Määttä, O., Dunne, E. M., Duplissy, J., Williamson, C., Barmet, P., Breitenlechner, M., Dommen, J., Donahue, N. M., Flagan, R. C., Franchin, A., Gordon, H., Hakala, J., Hansel, A., Heinritzi, M., Ickes, L., Jokinen, T., Kangasluoma, J., Kim, J., Kirkby, J., Kupc, A., Lehtipalo, K., Leiminger, M., Makhmutov, V., Onnela, A., Ortega, I. K., Petäjä, T., Praplan, A. P., Riccobono, F., Rissanen, M. P., Rondo, L., Schnitzhofer, R., Schobesberger, S., Smith, J. N., Steiner, G., Stozhkov, Y., Tomé, A., Tröstl, J., Tsagkogeorgas, G., Wagner, P. E., Wimmer, D., Ye, P., Baltensperger, U., Carslaw, K., Kulmala, M., and Curtius, J.: Experimental particle formation rates spanning tropospheric sulfuric acid and ammonia abundances, ion production rates, and temperatures, J. Geophys. Res.-Atmos., 121, 12377–12400, https://doi.org/10.1002/2015JD023908, 2016.

Laakso, A., Niemeier, U., Visioni, D., Tilmes, S., and Kokkola, H.: Dependency of the impacts of geoengineering on the stratospheric sulfur injection strategy – Part 1: Intercomparison of modal and sectional aerosol modules, Atmos. Chem. Phys., 22, 93–118, https://doi.org/10.5194/acp-22-93-2022, 2022.

Laakso, L., Gagné, S., Petäjä, T., Hirsikko, A., Aalto, P. P., Kulmala, M., & Kerminen, V. M.: Detecting charging state of ultra-fine particles: instrumental development and ambient measurements. Atmospheric Chemistry and Physics, 7(5), 1333-1345, 2007.

Lee, S. H., Gordon, H., Yu, H., Lehtipalo, K., Haley, R., Li, Y., & Zhang, R.: New particle formation in the atmosphere: From molecular clusters to global climate. Journal of Geophysical Research: Atmospheres, 124(13), 7098-7146, 2019.

Lee, S. H., Reeves, J. M., Wilson, J. C., Hunton, D. E., Viggiano, A. A., Miller, T. M., Ballenthin, J. O., and Lait, L. R.: Particle formation by ion nucleation in the upper troposphere and lower stratosphere, Science, 301, 1886–1889, https://doi.org/10.1126/science.1087236, 2003.

Li, M., Zhang, Q., Kurokawa, J.-I., Woo, J.-H., He, K., Lu, Z., Ohara, T., Song, Y., Streets, D. G., Carmichael, G. R., Cheng, Y., Hong, C., Huo, H., Jiang, X., Kang, S., Liu, F., Su, H., and Zheng, B.: MIX: a mosaic Asian anthropogenic emission inventory under the international

collaboration framework of the MICS-Asia and HTAP, Atmos. Chem. Phys., 17, 935–963, https://doi.org/10.5194/acp-17-935-2017, 2017.

Lockley, A., MacMartin, D., & Hunt, H.: An update on engineering issues concerning stratospheric aerosol injection for geoengineering. Environmental Research Communications, 2(8), 082001, 2020.

Lovejoy, E. R., Curtius, J., and Froyd, K. D.: Atmospheric ion-induced nucleation of sulfuric acid and water, J. Geophys. Res., 109, D08204, https://doi.org/10.1029/2003JD004460, 2004.

Luo, G., Yu, F., & Moch, J. M.: Further improvement of wet process treatments in GEOS-Chem v12. 6.0: impact on global distributions of aerosols and aerosol precursors. Geoscientific Model Development, 13(6), 2879-2903, 2020.

Martin, R. V., Jacob, D. J., Chance, K., Kurosu, T. P., Palmer, P. I., & Evans, M. J.: Global inventory of nitrogen oxide emissions constrained by space-based observations of NO2 columns. Journal of Geophysical Research: Atmospheres, 108(D17), 2003.

Mills, M. J., Richter, J. H., Tilmes, S., Kravitz, B., MacMartin, D. G., Glanville, A. A., Tribbia, J. J., Lamarque, J.-F., Vitt, F., Schmidt, A., and Gettelman, A.: Radiative and chemical response to interactive stratospheric sulfate aerosols in fully coupled CESM1 (WACCM), J. Geophys. Res., 122, 13061–13078, https://doi.org/10.1002/2017JD027006, 2017.

Murphy, D. M., Froyd, K. D., Bourgeois, I., Brock, C. A., Kupc, A., Peischl, J., Schill, G. P., Thompson, C. R., Williamson, C. J., and Yu, P.: Radiative and chemical implications of the size and composition of aerosol particles in the existing or modified global stratosphere, Atmos. Chem. Phys., 21, 8915-8932, 10.5194/acp-21-8915-2021, 2021.

Murray, L. T., Jacob, D. J., Logan, J. A., Hudman, R. C., & Koshak, W. J.: Optimized regional and interannual variability of lightning in a global chemical transport model constrained by LIS/OTD satellite data. Journal of Geophysical Research: Atmospheres, 117(D20), 2012.

Nadykto, A. B., & Yu, F.: Simple correction to the classical theory of homogeneous nucleation. The Journal of chemical physics, 122(10), 104511, 2005.

NASEM: Reflecting Sunlight: Recommendations for Solar Geoengineering Research and Research Governance. Washington, DC: The National Academies Press, 2021.

Pye, H. O., & Seinfeld, J. H.: A global perspective on aerosol from low-volatility organic compounds. Atmospheric Chemistry and Physics, 10(9), 4377-4401, 2010.

Richter, J., Visioni, D., MacMartin, D., Bailey, D., Rosenbloom, N., Lee, W., Tye, M., and Lamarque, J.-F.: Assessing Responses and Impacts of Solar climate intervention on the Earth system with stratospheric aerosol injection (ARISE-SAI), EGUsphere [preprint], https://doi.org/10.5194/egusphere-2022-125, 2022.

Rotman, D. A., Tannahill, J. R., Kinnison, D. E., Connell, P. S., Bergmann, D., Proctor, D., ... & Kawa, S. R.: Global Modeling Initiative assessment model: Model description, integration, and testing of the transport shell. Journal of Geophysical Research: Atmospheres, 106(D2), 1669-1691, 2001.

Shepherd, J. G.: Geoengineering the climate: science, governance and uncertainty. Royal Society, 2009.

Shi, Q., Jayne, J. T., Kolb, C. E., Worsnop, D. R., & Davidovits, P.: Kinetic model for reaction of ClONO2 with H2O and HCl and HOCl with HCl in sulfuric acid solutions. Journal of Geophysical Research: Atmospheres, 106(D20), 24259-24274, 2001.

Stettler, M.E.J., S. Eastham, S.R.H. Barrett (2011), Air quality and public health impacts of UK airports. Part I: Emissions, Atmos. Environ., 45, 5415-5424, 2011.

Stier, P., Feichter, J., Kinne, S., Kloster, S., Vignati, E., Wilson, J., Ganzeveld, L., Tegen, I., Werner, M., Balkanski, Y., Schulz, M., Boucher, O., Minikin, A., and Petzold, A.: The aerosol-climate model ECHAM5-HAM, Atmos. Chem. Phys., 5, 1125–1156, https://doi.org/10.5194/acp-5-1125-2005, 2005.

Sun, H., Eastham, S., & Keith, D.: Developing a Plume-in-Grid model for plume evolution in the stratosphere. Journal of Advances in Modeling Earth Systems, 14, e2021MS002816. https://doi.org/10.1029/2021MS002816, 2022.

Svensmark, J., Shaviv, N. J., Enghoff, M. B., & Svensmark, H.: The ION-CAGE code: A numerical model for the growth of charged and neutral aerosols. Earth and Space Science. 7, e2020EA001142. https://doi.org/10.1029/2020EA001142, 2020.

Thompson, C.R., Wofsy, S.C., Prather, M.J., Newman, P.A., Hanisco, T.F., Ryerson, T.B., Fahey, D.W., Apel, E.C., Brock, C.A., Brune, W.H., Froyd, K., Katich, J.M., Nicely, J.M., Peischl, J., Ray, E., Veres, P.R., Wang, S., Allen, H.M., Asher, E., Bian, H., Blake, D., Bourgeois, I., Budney, J., Bui, T.P., Butler, A., Campuzano-Jost, P., Chang, C., Chin, M., Commane, R., Correa, G., Crounse, J.D., Daube, B., Dibb, J.E., DiGangi, J.P., Diskin, G.S., Dollner, M., Elkins, J.W., Fiore, A.M., Flynn, C.M., Guo, H., Hall, S.R., Hannun, R.A., Hills, A., Hintsa, E.J., Hodzic, A., Hornbrook, R.S., Huey, L.G., Jimenez, J.L., Keeling, R.F., Kim, M.J., Kupc, A., Lacey, F., Lait, L.R., Lamarque, J.-F., Liu, J., McKain, K., Meinardi, S., Miller, D.O., Montzka, S.A., Moore, F.L., Morgan, E.J., Murphy, D.M., Murray, L.T., Nault, B.A., Neuman, J.A., Nguyen, L., Gonzalez, Y., Rollins, A., Rosenlof, K., Sargent, M., Schill, G., Schwarz, J.P., Clair, J.M.S., Steenrod, S.D., Stephens, B.B., Strahan, S.E., Strode, S.A., Sweeney, C., Thames, A.B., Ullmann, K., Wagner, N., Weber, R., Weinzierl, B., Wennberg, P.O., Williamson, C.J., Wolfe, G.M., and Zeng, L. 'The NASA Atmospheric Tomography (ATom) Mission: Imaging the Chemistry of the Global Atmosphere', Bulletin of the American Meteorological Society, 103: E761-E90. 2022.

Tilmes, S., Mills, M. J., Niemeier, U., Schmidt, H., Robock, A., Kravitz, B., Lamarque, J.-F., Pitari, G., and English, J. M.: A new Geoengineering Model Intercomparison Project (GeoMIP) experiment designed for climate and chemistry models, Geosci. Model Dev., 8, 43–49, https://doi.org/10.5194/gmd-8-43-2015, 2015.

Turco, R. P., Whitten, R. C., & Toon, O. B.: Stratospheric aerosols: Observation and theory. Reviews of Geophysics, 20(2), 233-279. doi: 10.1029/RG020i002p00233, 1982.

van der Werf, G. R., J. T. Randerson, L. Giglio, T. T. van Leeuwen, Y. Chen, B. M. Rogers, M. Mu, M. J. E. van Marle, D. C. Morton, G. J. Collatz, R. J. Yokelson, and P. S. Kasibhatla, Global fire emissions estimates during 1997–2016, Earth Sys. Sci. Data, 9, 697-720, 2017.

van Donkelaar, A., Martin, R.V., Leaitch, W.R., Macdonald, A.M., Walker, T.W., Streets, D.G., Zhang, Q., Dunlea, E.J., Jimenez, J.L., Dibb, J.E., Huey, L.G., Weber, R., Andreae, M.O.: Analysis of aircraft and satellite measurements from the Intercontinental Chemical Transport Experiment (INTEX-B) to quantify long-range transport of East Asian sulfur to Canada. Atmospheric Chemistry and Physics, 8(11), 2999-3014, 2008.

Vehkamäki, H., Kulmala, M., Napari, I., Lehtinen, K. E., Timmreck, C., Noppel, M., & Laaksonen, A.:. An improved parameterization for sulfuric acid–water nucleation rates for tropospheric

and stratospheric conditions. Journal of Geophysical Research: Atmospheres, 107(D22), AAC-3. doi: 10.1029/2002JD002184, 2002.

Weisenstein, D. K., Visioni, D., Franke, H., Niemeier, U., Vattioni, S., Chiodo, G., Peter, T., and Keith, D. W.: An interactive stratospheric aerosol model intercomparison of solar geoengineering by stratospheric injection of SO2 or accumulation-mode sulfuric acid aerosols, Atmos. Chem. Phys., 22, 2955–2973, https://doi.org/10.5194/acp-22-2955-2022, 2022.

Williamson, C., Kupc, A., Wilson, J., Gesler, D. W., Reeves, J. M., Erdesz, F., McLaughlin, R., & Brock, C. A.: Fast time response measurements of particle size distributions in the 3-60 nm size range with the nucleation mode aerosol size spectrometer. Atmospheric Measurement Techniques, 11(6), 3491-3509. doi:10.5194/amt-11-3491-2018, 2018.

Williamson, C. J., Kupc, A., Axisa, D., Bilsback, K. R., Bui, T., Campuzano-Jost, P., Dollner, M., Froyd, K. D., Hodshire, A. L., Jimenez, J. L., Kodros, J. K., Luo, G., Murphy, D. M., Nault, B. A., Ray, E. A., Weinzierl, B., Wilson, J. C., Yu, F. Q., Yu, P. F., Pierce, J. R., and Brock, C. A.: A large source of cloud condensation nuclei from new particle formation in the tropics, Nature, 574, 399–403, https://doi.org/10.1038/s41586-019-1638-9, 2019.

Williamson, C. J., Kupc, A., Rollins, A., Kazil, J., Froyd, K. D., Ray, E. A., Murphy, D. M., Schill, G. P., Peischl, J., Thompson, C., Bourgeois, I., Ryerson, T. B., Diskin, G. S., DiGangi, J. P., Blake, D. R., Bui, T. P. V., Dollner, M., Weinzierl, B., and Brock, C. A.: Large hemispheric difference in nucleation mode aerosol concentrations in the lowermost stratosphere at mid- and high latitudes, Atmos. Chem. Phys., 21, 9065–9088, https://doi.org/10.5194/acp-21-9065-2021, 2021.

Wofsy, S.C., S. Afshar, H.M. Allen, E.C. Apel, E.C. Asher, B. Barletta, J. Bent, H. Bian, B.C. Biggs, D.R. Blake, N. Blake, I. Bourgeois, C.A. Brock, W.H. Brune, J.W. Budney, T.P. Bui, A. Butler, P. Campuzano-Jost, C.S. Chang, M. Chin, R. Commane, G. Correa, J.D. Crounse, P. D. Cullis, B.C. Daube, D.A. Day, J.M. Dean-Day, J.E. Dibb, J.P. DiGangi, G.S. Diskin, M. Dollner, J.W. Elkins, F. Erdesz, A.M. Fiore, C.M. Flynn, K.D. Froyd, D.W. Gesler, S.R. Hall, T.F. Hanisco, R.A. Hannun, A.J. Hills, E.J. Hintsa, A. Hoffman, R.S. Hornbrook, L.G. Huey, S. Hughes, J.L. Jimenez, B.J. Johnson, J.M. Katich, R.F. Keeling, M.J. Kim, A. Kupc, L.R. Lait, K. McKain, R.J. Mclaughlin, S. Meinardi, D.O. Miller, S.A. Montzka, F.L. Moore, E.J. Morgan, D.M. Murphy, L.T. Murray, B.A. Nault, J.A. Neuman, P.A. Newman, J.M. Nicely, X. Pan, W. Paplawsky, J. Peischl, M.J. Prather, D.J. Price, E.A. Ray, J.M. Reeves, M. Richardson, A.W. Rollins, K.H. Rosenlof, T.B. Ryerson, E. Scheuer, G.P. Schill, J.C. Schroder, J.P. Schwarz, J.M. St.Clair, S.D. Steenrod, B.B. Stephens, S.A. Strode, C. Sweeney, D. Tanner, A.P. Teng, A.B. Thames, C.R. Thompson, K. Ullmann, P.R. Veres, N.L. Wagner, A. Watt, R. Weber, B.B. Weinzierl, P.O. Wennberg, C.J. Williamson, J.C. Wilson, G.M. Wolfe, C.T. Woods, L.H. Zeng, and N. Vieznor. 2021. ATom: Merged Atmospheric Chemistry, Trace Gases, and Aerosols, Version 2. ORNL DAAC, Oak Ridge, Tennessee, USA. https://doi.org/10.3334/ORNLDAAC/1925.

Yu, F., & Luo, G.: Simulation of particle size distribution with a global aerosol model: contribution of nucleation to aerosol and CCN number concentrations. Atmospheric Chemistry and Physics, 9(20), 7691-7710, 2009.

847   Yu, F., & Turco, R. P.: Ultrafine aerosol formation via ion-mediated nucleation. Geophysical
848   Research Letters, 27(6), 883-886. doi: 10.1029/1999GL011151, 2000.

849   Yu, F., Nadykto, A. B., Herb, J., Luo, G., Nazarenko, K. M., & Uvarova, L. A.: H_2SO_4–H_2O–NH_3
850   ternary ion-mediated nucleation (TIMN): kinetic-based model and comparison with CLOUD
851   measurements. Atmospheric Chemistry and Physics, 18(23), 17451-17474, 2018.

852   Yu, F., Nadykto, A. B., Luo, G., & Herb, J.: H_2SO_4–H_2O binary and H_2SO_4–H_2O–NH_3 ternary
853   homogeneous and ion-mediated nucleation: lookup tables version 1.0 for 3-D modeling
854   application. Geoscientific Model Development, 13(6), 2663-2670, 2020.

855   Zhang, R., Khalizov, A., Wang, L., Hu, M., & Xu, W.: Nucleation and growth of nanoparticles in
856   the atmosphere. Chemical reviews, 112(3), 1957-2011, 2012.
857